CLIMATOLOGY

Role of the stratosphere in the global mercury cycle

Alfonso Saiz-Lopez[1]*†, Carlos A. Cuevas[1]†, A. Ulises Acuña[1]†, Juan A. Añel[2,1], Anoop S. Mahajan[3], Laura de la Torre[2], Wuhu Feng[4,5], Juan Z. Dávalos[1], Daniel Roca-Sanjuán[6], Douglas E. Kinnison[7], Javier Carmona-García[1,6]‡, Rafael P. Fernandez[8], Qinyi Li[1,9], Jeroen E. Sonke[10], Aryeh Feinberg[1,11], Juan Carlos Gómez Martín[12], Julián Villamayor[1], Peng Zhang[13], Yanxu Zhang[14], Christopher S. Blaszczak-Boxe[15], Oleg Travnikov[16], Feiyue Wang[17], Johannes Bieser[18], Joseph S. Francisco[19], John M. C. Plane[4]

Mercury (Hg) is a global pollutant with substantial risks to human and ecosystem health. By upward transport in tropical regions, mercury enters into the stratosphere, but the contribution of the stratosphere to global mercury dispersion and deposition remains unknown. We find that between 5 and 50% (passing through the 400-kelvin isentropic surface and tropopause, respectively) of the mercury mass deposited on Earth's surface is chemically processed in the lower stratosphere. Our results show the stratosphere as a unique chemical environment where elemental mercury is efficiently converted to long-lived oxidized species. Subsequent downward transport contributes substantially to the oxidized mercury burden in the troposphere. The results show that the stratosphere facilitates the global dispersion of large amounts of mercury from polluted source regions to Earth's remote environments. We find that stratospheric transport is as important as tropospheric transport in interhemispheric mercury dispersion. Future projections suggest that expected changes in atmospheric circulation will increase the transport of mercury into the stratosphere.

INTRODUCTION

Over millennia, human activities have resulted in the emission of toxic elemental mercury into the atmosphere, where the element disperses globally because of its long atmospheric lifetime of several months (*1*, *2*). As a result, it is estimated that ~20% of total atmospheric mercury resides in the stratosphere (*3*, *4*), transported there by tropical deep convection. Eventually, mercury is oxidized to soluble or particle-reactive compounds across the atmosphere and deposited onto waters, soils, and ecosystems far away from its source regions, including in polar environments (*1*). While the health and ecosystem risks have been recognized, leading to the United Nations Minamata Convention on Mercury (*5*), which has been signed by more than 140 countries, the critical atmospheric processes that convert emitted elemental mercury [Hg(0)] into the more soluble and reactive oxidized mercury [Hg(I, II)] and the dispersal of both forms around the globe remain uncertain (*6*, *7*). Therefore, understanding mercury transport and chemistry in the troposphere as well as in the stratosphere is key to determining mercury inputs to Earth's ecosystems (*5*).

Ground-based measurements of atmospheric mercury are exhaustive and consistent (*8*–*11*), showing global levels of 1 to 1.7 ng m^{-3} (equivalent to 0.1 to 0.2 parts per trillion by volume), predominantly in the form of Hg(0). The surface Hg(0) concentrations are lower in the Southern Hemisphere (~1.0 ng m^{-3}) than in the Northern Hemisphere (~1.5 ng m^{-3}), although not as low as expected considering the 2.5-fold higher anthropogenic Hg emissions in the Northern Hemisphere. It has been suggested that this is caused by interhemispheric Hg exchange through the troposphere or by larger Southern Hemisphere marine Hg(0) emissions (*3*, *12*). Measurements of vertical profiles of Hg(0) or Hg(I, II) concentration in the troposphere and above the tropopause are scarce and lack calibration and, in the case of the oxidized forms, are likely biased low (*13*). Early aircraft measurements of aerosols between 5 and 19 km above the surface discovered the presence of non-meteoritic mercury in 50% of the analyzed particles, presumably in the form of Hg(I, II), up to 8 km above the tropopause, with increasing frequency at higher altitudes (*14*). Further measurements indicated the global presence of mercury-containing aerosol particles in and near the tropopause (*15*). Later, during the Intercontinental Chemical Transport Experiment-Phase B airborne campaign, which covered the 0.15- to 12-km altitude range, a low total mercury concentration (<0.5 ng m^{-3}) was reported in air masses with a stratospheric origin (*16*). Similarly, from measurements in which elemental and oxidized mercury in the gas phase and in particulate phases [Hg(P)] were differentiated at 6 to 7 km, it was concluded that Hg(0) is efficiently oxidized in the

[1]Department of Atmospheric Chemistry and Climate, Institute of Physical Chemistry Blas Cabrera, CSIC, 28006 Madrid, Spain. [2]Environmental Physics Laboratory (EPhysLab), Centro de Investigación Mariña (CIM-UVIGO), Universidade de Vigo, 32004 Ourense, Spain. [3]Centre for Climate Change Research, Indian Institute of Tropical Meteorology, Ministry of Earth Sciences, Pune 411008, India. [4]School of Chemistry, University of Leeds, Leeds, UK. [5]NCAS, University of Leeds, Leeds, UK. [6]Institut de Ciencia Molecular, Universitat de Valencia, 46071 Valencia, Spain. [7]NSF National Center for Atmospheric Research (NSF NCAR), Boulder, CO 80301, USA. [8]Institute for Interdisciplinary Science (ICB), National Research Council (CONICET), FCEN-UNCuyo, Mendoza 5501, Argentina. [9]Environment Research Institute, Shandong University, Qingdao 266237, China. [10]Géosciences Environnement Toulouse, CNRS/OMP/Université de Toulouse, 31400 Toulouse, France. [11]Institute for Data, Systems and Society, Massachusetts Institute of Technology, Cambridge, MA 02139, USA. [12]Instituto de Astrofísica de Andalucía, CSIC, 18008 Granada, Spain. [13]School of Atmospheric Sciences, Nanjing University, Nanjing, China. [14]Department of Earth and Environmental Sciences, Tulane University, New Orleans, LA 70118, USA. [15]Earth, Equity, and Environment Department, Howard University, Washington, DC 20059, USA. [16]Department of Environmental Sciences, Jožef Stefan Institute, Jamova cesta 39, 1000 Ljubljana, Slovenia. [17]Centre for Earth Observation Science, and Department of Environment and Geography, University of Manitoba, Winnipeg, MB R3T 2N2, Canada. [18]Helmholtz-Zentrum Geesthacht, Institute of Coastal Research, Max-Planck-Strasse 1, 21502 Geesthacht, Germany. [19]Department of Earth and Environmental Science and Department of Chemistry, University of Pennsylvania, Philadelphia, PA 19104, USA.
*Corresponding author. Email: a.saiz@csic.es
†These authors contributed equally to this work.
‡Present address: Centre for Computational Chemistry, School of Chemistry, University of Bristol, Bristol BS8 1TS, UK.

stratosphere (*17*). Recently, a large set of airborne mercury measurements in the upper troposphere/lower stratosphere (UTLS) from the In-service Aircraft for a Global Observing System (IAGOS) - Civil Aircraft for the Regular Investigation of the Atmosphere Based on an Instrument Container (CARIBIC) observatory showed gas-phase Hg(0) concentrations in the range of 0.25-0.7 ng m^{-3} up to 4 km above the tropopause (*18*). A larger contribution of oxidized species to the total mercury budget in the UTLS and partitioning between gas phase and particulate mercury was also reported (*18*). Although these observations that go back two decades have revealed active mercury cycling in the stratosphere, the contribution of stratospheric chemistry and transport to the global Hg dispersion and deposition remains unquantified.

Global and regional mechanistic models of atmospheric chemistry and transport are complex but indispensable tools for understanding the critical atmospheric component of the biogeochemical mercury cycle [see (*3*) and references therein]. In this regard, previous analyses have focused on the chemistry and transport of mercury within the troposphere (*2*, *3*, *12*, *19*–*25*). In some cases, the analysis also included the stratosphere, but only as an extension of the chemical processes that are characteristic of the troposphere (*3*, *4*, *17*, *19*). Here, we build a new comprehensive whole atmosphere model that, in addition to state-of-the-art tropospheric mercury emissions and photochemistry, also incorporates mercury chemical and transport processes specific to the stratosphere. We quantify the contribution of the stratosphere to mercury chemical transformation, global and interhemispheric transport, and deposition on the Earth's surface. The model reproduces well the observed vertical profiles of mercury. The results show that transport and the unique mercury redox chemistry in the stratosphere, followed by subsequent downward transport into the troposphere, constitute a key contribution to the net global surface deposition of mercury and determine the geographical pattern of mercury deposition. We uncover a previously unknown global circulation pathway via the stratosphere that transports mercury from anthropogenic source regions to remote environments, including polar regions.

RESULTS

Chemistry of mercury in the stratosphere

The role of the stratosphere in the global mercury cycle is investigated using the Whole Atmosphere Community Climate Model (WACCM) (see Materials and Methods for model description and validation). In contrast to previous work, we implemented mercury chemical mechanisms specific to the stratosphere in WACCM (see the "Mercury chemistry in WACCM" section), briefly outlined below.

Oxidation of elemental mercury in the troposphere and lower stratosphere is explained by initial reactions (reaction 1) with Br atoms and, to a lower extent, with less abundant Cl atoms and less reactive OH radicals (*3*, *20*, *21*, *24*, *26*, *27*)

$$\begin{aligned} &\mathrm{Hg(0)+X+M \leftrightarrow XHg(I)+M} \\ &\mathrm{X=Cl, Br, OH;\quad M=air\ molecule} \end{aligned} \tag{1}$$

In the upper stratosphere, above the ultraviolet (UV)–absorbing ozone layer, the additional, fast photosensitized reaction of excited mercury atoms with molecular oxygen triggered by 254-nm radiation (reaction 2) becomes the dominant oxidation pathway (*26*)

$$\mathrm{Hg(0) + O_2 + h\upsilon\,(254\ nm) \rightarrow Hg^* + O_2 \rightarrow HgO + O} \tag{2}$$

These first-step oxidation reactions are counterbalanced by gas phase reduction processes of the newly formed reaction products. Some of them are thermal dissociation reactions, while another important group is made up of photodissociation reactions back to elemental mercury (*2*, *23*, *28*). Secondary reactions of the intermediates XHg(I) not only with O_3 (*2*, *29*) but also with NO_2, HO_2, etc., yield lastly a series of Hg(II) compounds with different photostabilities, prominently $HgCl_2$, HgBrOH, $Hg(OH)_2$, HgClOH, and $HgBr_2$ (see details below and in the "Mercury chemistry in WACCM" section).

Our coupled troposphere-stratosphere results are in good agreement with observations of mercury concentration vertical profiles (Fig. 1D). Note that the quantification of vertical concentration profiles of mercury species shown in Fig. 1D may have considerable uncertainties due to technical limitations thoroughly discussed recently (*13*). In addition, these profiles reveal the central role that the stratosphere plays in mercury cycling, showing large changes in the chemical lifetime of elemental mercury from the surface to the top of the stratosphere (fig. S1). We find that the largest mixing ratios of oxidized mercury Hg(I, II) in the atmosphere, concomitant with the lowest of Hg(0), are located in the lower stratosphere, in a layer ~5 km thick above the tropopause (Fig. 1). The vertical profiles show positive excursions of Hg(I, II) where chemical processes oxidize Hg(0), and vice versa (Fig. 1B), thereby revealing the lower stratosphere as a hotspot for Hg(I, II) formation [i.e., with a smaller Hg(0)/Hg(I, II) ratio; Fig. 1C].

The reason for the enrichment in mercury oxidation products in the lower stratosphere is the shift in the balance between the oxidation reactions of Hg(0) and the photoreduction of the resulting Hg(I, II) species, which specifically favors the formation of $HgCl_2$, the most stable atmospheric form of oxidized mercury (*28*) (Materials and Methods, fig. S2 and table S1). In the lower stratosphere, the first-step reactions of Hg(0) with Br and OH radicals are two orders of magnitude faster than the reaction with Cl atoms (fig. S3). However, the rates of photoreduction back to Hg(0) of the resulting products of Br/OH oxidation are also much faster than that of $HgCl_2$, the product of chlorine-mediated mercury oxidation (fig. S2). In addition, above the mid-stratosphere, the recently reported photosensitized oxidation pathway (*26*) also produces $HgCl_2$ (table S2). Hence, the formation of photostable $HgCl_2$ in the stratosphere allows its accumulation and transport downward into the global troposphere, becoming the dominant oxidized species throughout most of the atmosphere (figs. S2 and S4). Overall, the higher photostability of $HgCl_2$ makes the net oxidation of mercury in the stratosphere more efficient than in the troposphere (fig. S2), despite the longer chemical lifetime of Hg(0) in the stratosphere (fig. S1). The model results show that the downward transport of stratospheric $HgCl_2$ into the troposphere contributes 51 ± 15% of the total oxidized mercury in the global troposphere, thereby helping to explain the underestimates of oxidized mercury in models that only include tropospheric chemistry (*2*).

In summary, these results show that the lower stratosphere functions as a global chemical sink of Hg(0) and a source of photostable Hg(I, II) compounds, mainly $HgCl_2$. The efficient chemical conversion of Hg(0) to Hg(I, II) means that the lower stratosphere contains the highest mixing ratios of oxidized mercury in the global atmosphere. The model predicts the existence of a layer of enhanced oxidized mercury in the lower stratosphere extending globally from north to south (Fig. 1B).

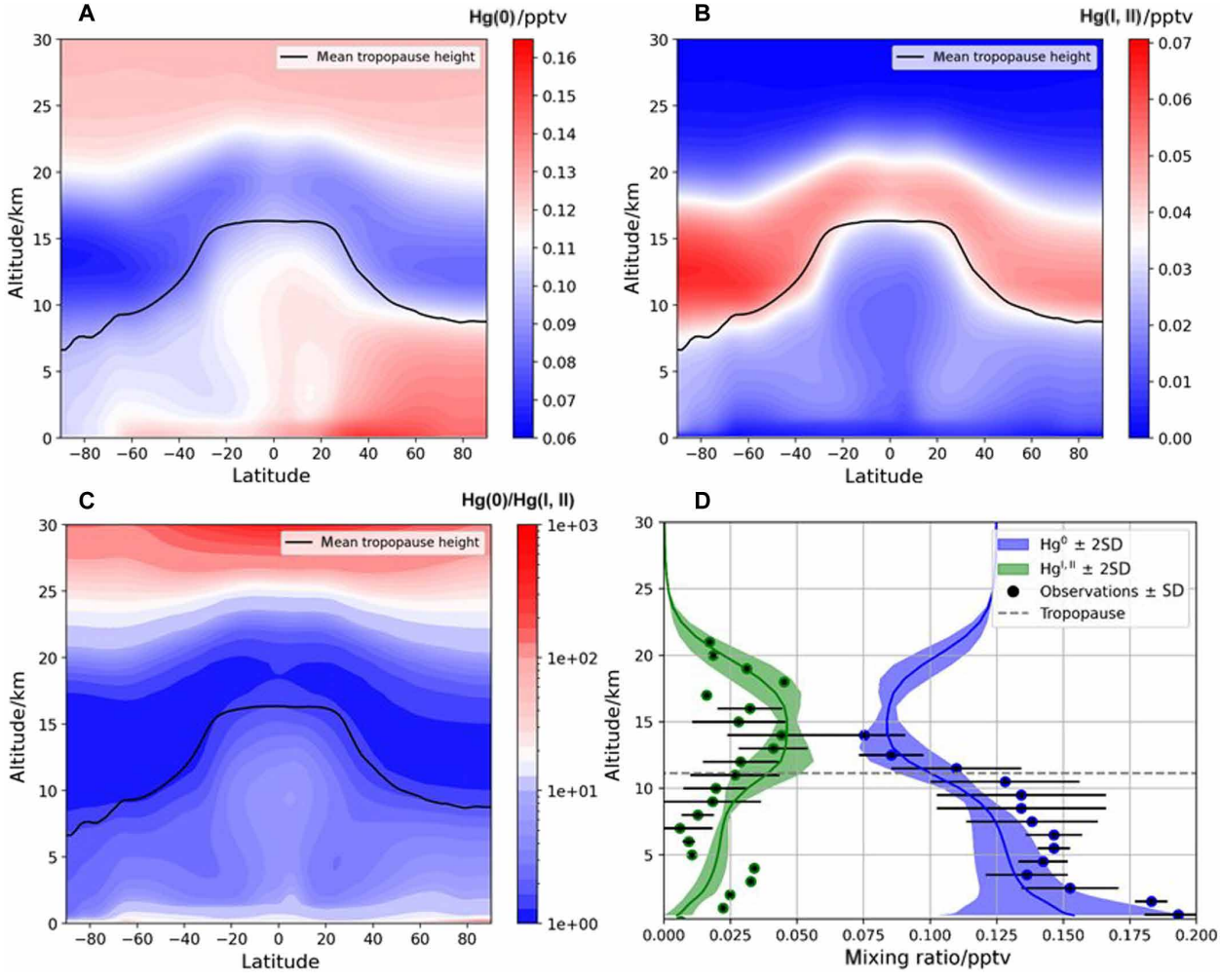

Fig. 1. Modeled 2005–2014 averaged zonal-mean mercury vertical atmospheric concentration. (**A**) Elemental [Hg(0)], (**B**) oxidized mercury [Hg(I, II)], (**C**) Hg(0)/Hg(I, II) ratio, and (**D**) observed and modeled vertical Hg(0) and Hg(I, II) profiles for 30°N to 60°N. The black line in (A) to (C) indicates the average tropopause height. The definition of tropopause is based on the lapse rate or rate of decrease of temperature with height (*56*). (D) Modeled vertical profiles of Hg(0) and Hg(I, II) in parts per trillion by volume (pptv), averaged in the 30°N to 60°N region [shaded areas represent two times the spatiotemporal standard deviation (SD), ±2σ], together with measured observations (black dots including SD, ±1σ), see the "Model validation" section. The model results show a layer in the lower stratosphere with the lowest Hg(0) and highest Hg(I, II) mixing ratios, due to efficient oxidation chemistry.

Budgets of atmospheric mercury

We estimate a mean atmospheric (troposphere + stratosphere) mercury lifetime against surface deposition of 8.2 months, 21% longer than the lifetime of mercury in the troposphere (6.8 months). Therefore, cycling and transport in the stratosphere increases the effective lifetime of mercury in the global atmosphere. The model shows that ~17 ± 4% of the total atmospheric mercury load is in the stratosphere, with a total Hg mass of 809 ± 202 Mg [553 ± 138 Mg Hg(0), 199 ± 50 Mg Hg(I, II), and 57 ± 14 Mg Hg(P)]. In comparison, the troposphere contains 3909 ± 977 Mg [3384 ± 846 Mg Hg(0), 507 ± 127 Mg Hg(I, II), and 18 ± 4 Mg Hg(P)]. Therefore, although most of the atmospheric Hg mass is present in the troposphere, the relative abundance of Hg(I, II) compared to that of Hg(0) is higher in the stratosphere. In the troposphere, ~86 ± 21% of the Hg mass is in the less reactive elemental form [13 ± 3% Hg(I, II) and 1% Hg(P)]. In the stratosphere, the elemental form represents a lower fraction of ~68 ± 17% [25 ± 6% Hg(I, II) and 7 ± 2% Hg(P)]. The more efficient net oxidation in the stratosphere is key to understand the global deposition of Hg.

Stratospheric contribution to oxidized mercury deposition

To track the mercury species that enter the stratosphere, we have followed the methodology used in Shah and Jaeglé (*4*) (see the "Mercury transport in the stratosphere" section). In our "base" simulation, Hg species are tagged when they reach the first layer above the tropopause (1 to 1.5 km above the tropopause). To estimate a range of uncertainty in the stratospheric contribution to mercury deposition, two sensitivity simulations were performed tagging Hg at two different layers of the atmosphere. The first sensitivity represents the upper limit and tags Hg species directly at the tropopause, while the second simulation tags Hg in the 400-K isentropic surface (i.e., at a higher height, representing mercury transported further into the stratosphere over longer timescales) to estimate a lower limit for stratospheric mercury deposition in the surface. Averaged

globally, ~30 ± 8% of the deposited mercury passes through the lower stratosphere in the base simulation (first layer above the tropopause). This contribution increases to 50 ± 12% when considering Hg passing through the tropopause layer and decreases to 5 ± 1.5% when considering only Hg that reached the 400-K isentropic surface. The total global deposition of mercury [wet and dry deposition of Hg(II) and Hg(P)] along with the relative fractional contribution of the troposphere and the stratosphere for the base simulation is shown in Fig. 2. Globally, 6920 ± 1730 Mg year^{-1} of oxidized mercury is deposited onto the Earth's surface. Of this amount, 4870 ± 1217 Mg year^{-1} (70 ± 17%) of the deposited mass is oxidized only in the troposphere, while 2050 ± 512 Mg year^{-1} (30 ± 8%) is cycled through the first layer above the tropopause (1 to 1.5 km above the tropopause). Note that this relative contribution of the stratosphere to the deposited mass of mercury is larger than the ~17 ± 4% of total atmospheric mercury that resides in the stratosphere. This is a consequence of the more efficient mercury oxidation to photostable products ($HgCl_2$) in the lower stratosphere, resulting in relatively more Hg(0) converted into soluble Hg(I, II) compounds within this region, which then subsides to the troposphere and eventually deposits on the Earth's surface. This finding reveals the large impact of the efficient stratospheric mercury oxidation on global mercury deposition, despite it containing only a small fraction of the total atmospheric mercury mass.

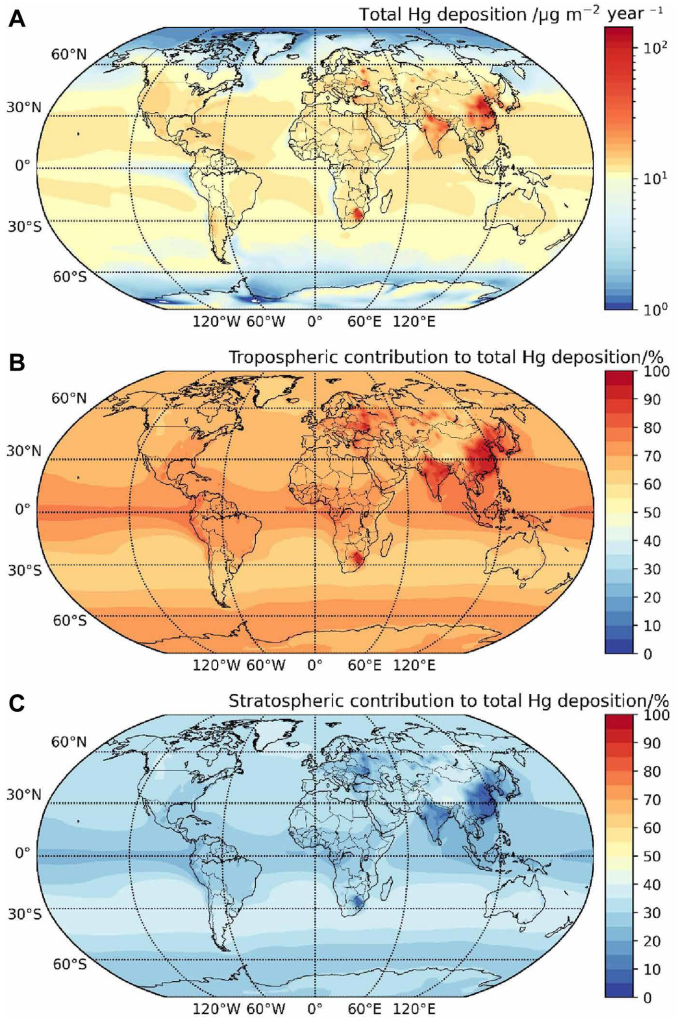

Fig. 2. Modeled 2005–2014 average total mercury deposition [wet and dry deposition of Hg(II) and Hg(P)]. (**A**) The total Hg deposition rate (in micrograms per square meter per year), with maxima close to the source regions, such as in eastern Asia, southern Asia, southern Africa, and eastern Europe; (**B**) tropospheric contribution to the total deposition; and (**C**) the stratospheric contribution. This stratospheric contribution accounts for mercury entering into the stratosphere where it is oxidized, transported, and deposited to remote regions. The tropospheric contribution represents only deposited mercury cycled below the tropopause, and hotspots in (B) correspond to local emissions with deposition of tropospheric mercury in or close to emissions sources.

While the transport of mercury to the stratosphere is known to occur through the tropics and midlatitudes, predominantly in the Hg(0) form (*18*), the impact of stratospheric cycling is especially noticeable in the deposition of mercury in remote regions far from emission sources (Fig. 2 and fig. S5). Most of the total mercury deposition occurs in the Northern Hemisphere, where the main sources are located. Deposition over the regions close to anthropogenic sources is dominated by tropospheric cycling, whereas deposition over regions farther away from the sources is controlled by cycling and transport in both the troposphere and stratosphere. Following the established global circulation patterns (*30*), the subsidence of mercury from the stratosphere into the troposphere occurs mainly in mid- to high latitudes. This result highlights the important role of the stratosphere in transporting Hg to remote environments. Our results show that 33 ± 8% and 29 ± 7% of the deposited mercury in the Arctic and Antarctic comes from the stratosphere, mainly in the form of $HgCl_2$ and $HgBr_2$ (Fig. 2 and table S3). In this regard, it is remarkable that past observations have shown that half of the atmospheric samples of oxidized mercury recovered in Svalbard (79°N) contain Cl/Br compounds of the metal (*31*).

Furthermore, our finding of the strong impact of stratospheric oxidation on global surface deposition, especially in the Arctic, can explain the recent observation (*32*) of large mass-independent fractionation (MIF) of even-mass-number isotopes of mercury (e.g., ^{200}Hg) in high altitude, >6000 m air masses. To date, the only known process that can result in the even-MIF of mercury is the UV radiation at 254 nm producing excited triplet Hg atoms [Hg(^{3}P)] and the subsequent formation of mercuric oxides (*33*, *34*). Such reactions are only possible in the stratosphere because optical absorption by the ozone layer prevents UV-C (200 to 280 nm) wavelengths from reaching the troposphere. Our results therefore help to explain why substantial even-MIF of mercury occurs in the atmosphere (e.g., in the air, cloud water, and precipitation) and why the highest degree of fractionation is found in the Arctic (*32*, *34*, *35*).

Interhemispheric mercury transport via the stratosphere

Our simulations indicate that mercury interhemispheric transport in the stratosphere should be considered in the understanding of the observed low atmospheric Hg concentration gradient between the Northern (~1.5 ng m^{-3}) and Southern Hemispheres (*36*, *37*) (~1.0 ng m^{-3}), although anthropogenic mercury emissions are ~2.5 times higher in the Northern Hemisphere than in the Southern Hemisphere (*36*–*38*). Past observations in South America have linked an increase in observed mercury concentrations to interhemispheric mercury exchange via the upper troposphere over the tropical Pacific Ocean (*39*). Our model results indicate that mercury exchange from the Northern to the Southern Hemisphere occurs primarily via the stratosphere, reducing the interhemispheric mercury gradient.

We ran a model scenario using only emissions in the Northern Hemisphere (see Materials and Methods) to quantify the impact of interhemispheric transport through the stratosphere (fig. S6). The results of our base simulation show that ~52% of Northern Hemisphere emissions that contribute to mercury deposition in the Southern Hemisphere are transported via the stratosphere compared to ~48% transported through the troposphere (fig. S6). Hence, stratospheric transport is as important as tropospheric transport for mercury dispersion from the Northern to the Southern Hemisphere.

DISCUSSION

Implications for atmospheric mercury research

Our results show that the stratosphere is a critical region of the atmosphere for a better understanding of the distribution, cycling, and fate of mercury in the atmosphere and, ultimately, for more precise quantification of the global input of atmospheric mercury into the Earth's surface ecosystems (Fig. 3). This understanding has substantial consequences for ecosystem exposure to mercury contamination, with resultant impacts on human and wildlife health.

We suggest that the stratosphere functions as a "conveyor belt" where large amounts of mercury are chemically processed and transported from over Earth's polluted source regions to remote environments. Stratospheric circulation contributes to the dispersion of mercury across the global atmosphere and its efficient conversion from Hg(0) to Hg(I, II), which is eventually deposited onto the surface. We find that, on a global basis, between 5 and 50% (passing through the 400-K isentropic surface and tropopause, respectively) of atmospheric mercury is chemically processed within the lower stratosphere before being deposited onto the surface.

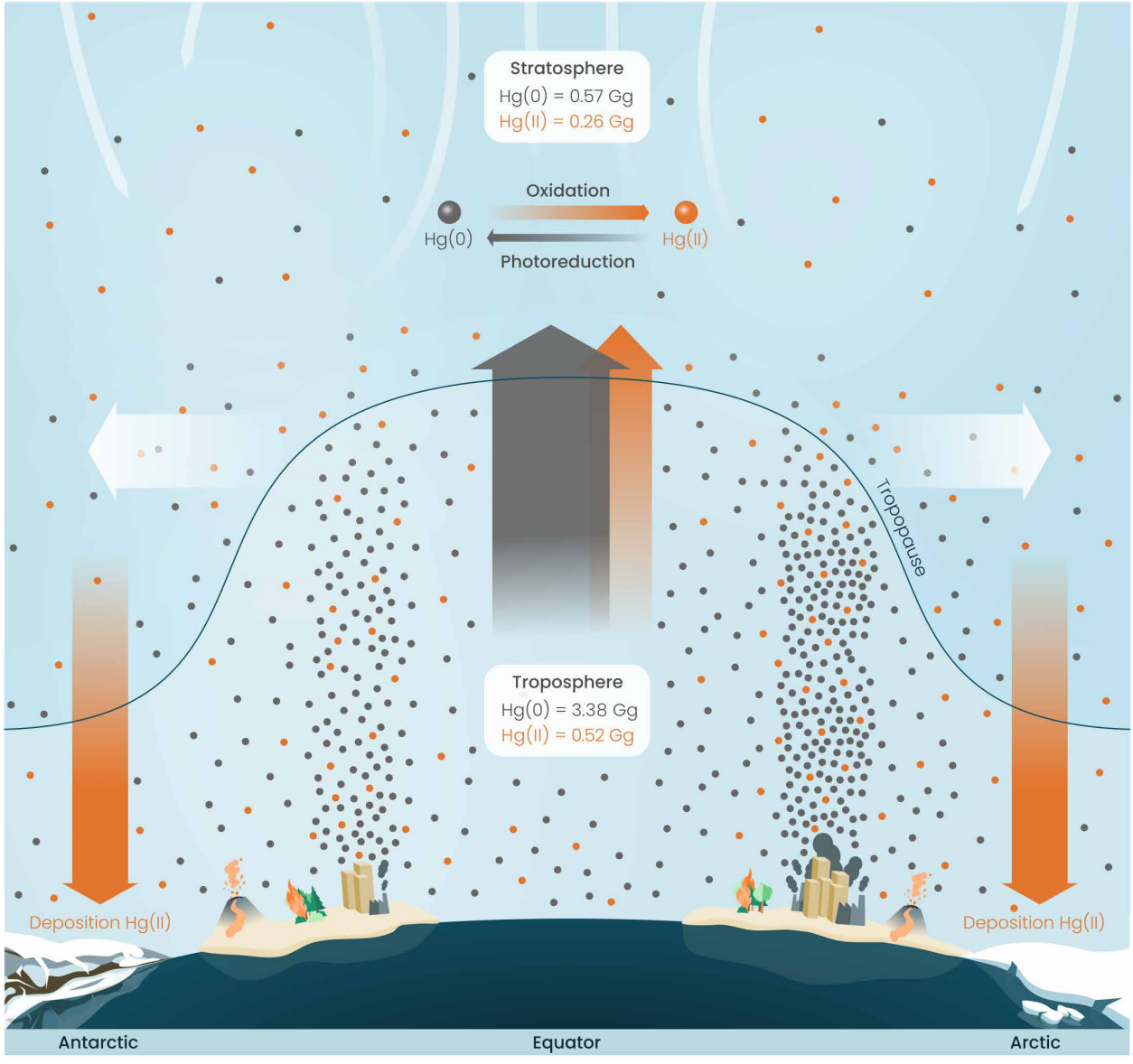

Fig. 3. Conceptual representation of the exchange of mercury across the tropopause and surface deposition fluxes. The transport of mercury to the stratosphere is predominantly as elemental Hg(0) (black dots) through the tropics and midlatitudes (20° to 60°), while most of the stratospheric mercury subsides back into the troposphere at midlatitudes and the polar regions, with a larger fraction of oxidized mercury (orange dots).

This stratospheric contribution to mercury surface deposition can be even larger in remote environments, particularly in the southern midlatitudes. Stratospheric circulation can also be as important as tropospheric dispersion for mercury transport from the Northern to the Southern Hemisphere.

Furthermore, the crucial role of stratospheric circulation in the dispersion and surface deposition of mercury will have important implications for the future. In response to global warming, the Brewer Dobson circulation is projected to strengthen (*40*, *41*) and stratospheric meridional transport velocities from tropics to polar regions to increase (*42*), resulting in important changes in the role of the stratosphere in mercury deposition under climate change. To assess the significance of this, we ran a future projection to the end of the 21st century under the representative concentration pathway RCP8.5 (*43*) (Future RCP8.5 2080-2099 scenario described in Materials and Methods). The results indicate a global increase of 12% in the contribution of stratospheric mercury to the total Hg(I, II) deposition by the end of the 21st century relative to the present day. This widespread increase is particularly accentuated over the tropical oceanic surface and at high latitudes (fig. S7). Hence, under ongoing climate change, it is expected that our current estimate of mercury deposition due to stratospheric cycling will increase in the future with associated changes on the spatial distribution of surface deposition over time, stressing the need for enhanced emissions reductions to prevent the increased risk of mercury poisoning under climate change.

Atmospheric Hg models are used to attribute Hg deposition to source regions and activities (*44*), as well as to project future mercury deposition patterns based on emissions and climate scenarios (*45*). Many existing mercury models do not adequately resolve stratospheric transport of mercury, and none have considered stratosphere-specific reactions in their chemical mechanism (*46*). Thus, the findings presented here on the importance of the stratosphere for the long-range transport, oxidation, and deposition of mercury highlight previously unexplored directions for the improvement of these models. The stratospheric transport of mercury from anthropogenic source regions to the polar regions, where a large fraction of the deposited mercury comes from the stratosphere, challenges the decades-old paradigm on the transport of mercury to the Arctic and Antarctic regions via the troposphere, where transport through the stratosphere was not considered. Therefore, future mercury assessments need to consider the interannual variability and trends in stratospheric dynamics, as these drivers could mediate the impacts of mercury emissions on surface ecosystems. We conclude that research efforts in atmospheric mercury cycling, which traditionally focused on the troposphere, should now include mercury chemical processing and transport in the stratosphere.

MATERIALS AND METHODS

Mercury chemistry in WACCM

The state-of-the-art redox chemical mechanism used in the present simulations has been described in detail in a recent publication (*26*); a list of reactions included in WACCM is provided in table S2. This mechanism incorporates evaluated rate constants and the most recent theoretical and experimental data on atmospheric gas-phase mercury chemistry and photochemistry. The best available evidence suggests that the direct oxidation of Hg(0) by O_3 to HgO is negligible (*6*). Accordingly, the oxidation of elemental mercury Hg(0) in the troposphere and lower stratosphere, below the ozone layer, is initiated by recombination with atomic Br, OH radicals, and, to a lesser extent, Cl atoms (*2*, *3*, *26*). The resulting short-lived XHg(I) (X = Br, OH, and Cl) intermediates formed in this way are further oxidized preferentially (*29*, *47*) to XHgO(II) by reaction with O_3 and to XHgY(II) by reaction with Y = NO_2, HO_2, OH, BrO, ClO, Br, and Cl. The major Hg(II) species, BrHgOH and $Hg(OH)_2$, are formed by reactions between XHgO and methane (*48*). Mercury oxidation is balanced by reduction reactions including XHgO + CO (*49*) and photoreduction (*2*, *23*, *28*, *50*, *51*) of Hg(I) and Hg(II) compounds. The particulate mercury formation has been implemented as an uptake of highly soluble Hg(II) compounds on stratospheric aerosols. This uptake converts gaseous Hg(II) to particulate Hg(P), which is not photolyzed back to the gas phase and has been implemented assuming an uptake coefficient $\gamma = 1 \times 10^{-4}$ for all Hg species ($HgBr_2$, HgBr, HgCl, HgBrOH, $HgBrNO_2$, HgBrOOH, HgBrCl, $HgCl_2$, HgClO, HgO, and HgOH).

Dry deposition for $HgBr_2$, $HgBrNO_2$, HgBrOH, HgBrOOH, $HgCl_2$, Hg(P), HgBrCl, HgClO, $Hg(OH)_2$, HgClOH, HgOHONO, HgOHOOH, HgOHO, HgClONO, and HgClOOH has been implemented, with 1 cm s^{-1} as deposition velocity for all species (*52*). Wet deposition for $HgBr_2$, $HgBrNO_2$, HgBrOH, HgBrOOH, $HgCl_2$, HgO, HgBrOCl, Hg(P), HgBrCl, HgClO, $Hg(OH)_2$, HgClOH, HgOHONO, HgOHOOH, HgOHO, HgClONO, and HgClOOH has been implemented following the scheme from Neu and Prather (*53*) for HNO_3. The Henry's law solubility constants for these mercury species (*54*) are shown in table S4.

In the mid- to upper-stratosphere, above the ozone layer (>25 km), an additional oxidation pathway is initiated by photosensitized chemistry (*26*), where in the absence of a strong absorption in the near-UV by ozone, ground state mercury $Hg(^1S_0)$ is excited to highly reactive $Hg(^3P_1)$ by absorption at 253.7 nm (table S2). The reaction of $Hg(^3P_1)$ with O_2 to form HgO competes with the relaxation of $Hg(^3P_1)$ by spontaneous emission and collisions with air molecules. This is most likely the origin of Hg mass-independent even-isotope fractionation (*34*). The reaction between HgO and HCl, an abundant species in the stratosphere, to yield HgCl competes favorably with HgO dissociation and the reductive reaction with ozone. Then, HgCl reacts with ozone to yield ClHgO, and, after further reactions with HCl, it lastly produces $HgCl_2$. Therefore, the photosensitized oxidation is an additional path to the most stable atmospheric form of oxidized mercury.

Mercury transport in the stratosphere

We have used a tagging technique to identify the Hg atoms in any form [Hg(0), Hg(I, II), and Hg(P)] that enter the stratosphere. This methodology follows that used by Shah and Jaeglé (*4*). In our base simulation, mercury species are tagged when they reach the first layer above the tropopause (1 to 1.5 km above the tropopause). Then, the chemical and physical processes that tagged species undergo are the same as for those that did not reach the stratosphere (untagged species). This method allows the tracking of tagged species globally and their relative contribution to global Hg budgets and surface deposition. In addition, two sensitivity simulations were conducted which involved tagging at two different layers of the atmosphere to estimate a range of uncertainty in the stratospheric contribution to mercury deposition. In the first model run, which can be considered as an upper limit, the stratospheric tag was applied

at the tropopause height, while, in a second sensitivity experiment, the tag was applied at the 400-K isentropic surface.

Note that the tropopause is computed here following the World Meteorological Organization definition (*55*): "The first tropopause is defined as the lowest level at which the lapse rate decreases to 2°C/km or less, provided also the average lapse rate between this level and all the higher levels within 2 km does not exceed 2°C/km." In this work, we use its monthly mean altitude, an output field from the model (TROP_Z), using a widely used implementation (*56*).

In addition to this tagging approach and to ensure its consistency, we also calculated stratosphere-troposphere exchange (STE) using two different techniques, which agree with the corresponding values obtained from the tagging approach:

1) The Appenzeller *et al.* (*57*) formalism to compute cross-tropopause mass transport

2) Using the variables for mass flux variation internally computed by WACCM4, taking into account the terms for advective transport, chemical transport, and vertical diffusion, all of them computed using the transformed Eulerian mean (*58*–*60*)

With this methodology, we obtain a global deposition of stratospheric mercury of 349 Mg year^{-1} (5% of the total mass), in agreement with our second sensitivity run tagging at the 400-K isentropic. The STE results of this second sensitivity are consistent with previous studies about STE considering the region between the tropopause and the 380-K isentropic surface (*61*, *62*).

WACCM configuration

In this work, we used the WACCM version 4 (WACCM4) (*63*), a fully coupled state-of-the-art interactive chemistry-climate model (*64*). The model setup, with a spatial resolution of 1.9° latitude × 2.5° longitude and 88 vertical levels (~1.4-km vertical resolution in the lower stratosphere), is based on the specified dynamics version of WACCM4 (SD-WACCM), including reanalysis for temperature, zonal and meridional winds, as well as surface pressure fields from the Modern-Era Retrospective Analysis for Research and Applications (MERRA2) (*65*–*67*). The standard WACCM chemical scheme includes the O_x, NO_x, HO_x, ClO_x, and BrO_x chemical families, along with gas-phase and heterogeneous reactions on liquid binary and ternary sulfate polar stratospheric cloud particles, as well as solid nitric acid trihydrate and water ice polar stratospheric particles (*68*). The model (*69*) also incorporates an updated halogen chemistry scheme for chlorine, bromine, and iodine. This version of the WACCM model was used in previous stratospheric studies (*26*, *70*).

WACCM4 (in free runs and with nudged data) has been broadly used to evaluate troposphere-stratosphere exchanges in previous work (*71*–*76*), which supports its suitability for this study. Previous studies based on WACCM show that the STE in the tropics is dominated by advection, while, in the extra-tropics, the exchange of air masses is dominated by eddy transport (*72*). WACCM also succeeds in representing the temporal evolution of STE and the associated mechanisms in agreement with other models (*73*). In addition, our simulations have been tested to represent the climatological STE reported by previous works (*73*, *74*, *77*). This is shown in fig. S8, which includes the modeled averaged zonal mean of stratospheric ozone tracer (O_3ST). O_3ST is the amount of ozone photochemically produced in the stratosphere which is transported and destroyed in the troposphere.

The benchmark WACCM4 troposphere-stratosphere-mesosphere-and-lower-thermosphere chemical scheme was updated to include previous developments of short-lived (SLH) tropospheric halogen chemistry already implemented in the Community Atmosphere Model with Chemistry (CAM-Chem4) version of the Community Earth System Model (CESM1) (*26*, *78*–*81*). This includes the offline emission of oceanic SLH chloro-, bromo-, and iodo-carbons; the online computation of the sea-salt aerosol (SSA) dehalogenation source due to the effective uptake of chloride and bromide from SSA; and the heterogeneous reactivation of inorganic halogen reservoirs on the surface of ice crystals in the upper troposphere (*79*, *81*, *82*). For the particular case of iodine chemistry, additional sources of inorganic iodine (in the form of HOI and I_2) due to the ozone-driven oxidation of aqueous iodide occurring at the ocean surface were also included (*83*–*86*).

We used the speciated anthropogenic Hg emission inventory by Zhang *et al.* (*87*), which is an improved global inventory that incorporated the release of mercury from commercial products and emission controls during coal combustion. The total anthropogenic emissions were about 2300 Mg year^{-1}, with 65% Hg(0) and 35% Hg(II) and Hg(P). We obtained the natural/recycling emissions by averaging a 5-year simulation in GEOS-Chem v11 (*24*) coupled with the MITgcm three-dimensional oceanic model (*88*). The reemissions from ocean and soil were about 3200 and 930 Mg year^{-1}, respectively, within the current estimates for mercury budget (*89*). We interpolated these emissions from the original resolution to 1.9° × 2.5° for WACCM. Note that the estimated annual flux of meteoric material arriving at Earth is 16,600 kg/year^{-1} (uncertainty around 50%) (*90*), which, together with a median Hg concentration in meteorites of 203 μg kg^{-1} (interquartile range, 40 to 965) (*91*, *92*), results in an amount of about 3.4 g of Hg, which is millions of times smaller than tropospheric Hg inputs into the stratosphere. Therefore, our model configuration does not include this negligible amount of mercury (*93*) deposited from meteoric material.

To identify the transport and cycling of mercury through the stratosphere, all Hg species reaching a specific layer (depending on the simulation: tropopause, 1 to 1.5 km above the tropopause, 400 K isentrope) have been tagged in the model as "stratospheric mercury" (see the "Mercury transport in the stratosphere" section for details). In this way, we can track any mercury atom in Hg(0), Hg(I, II), or Hg(P) forms that has entered the stratosphere and their subsequent chemical transformations until they undergo surface deposition. This allows us to differentiate between the budget and deposition of tropospheric mercury from the budget and deposition of mercury transported and cycled through the stratosphere.

We conducted three runs for this study following on our base simulation and according to time and mercury emissions:

1) Present-day scenario: This is the base SD-WACCM simulation and includes all global Hg emissions inventories. This simulation for the 2005–2014 time period has been run with a spin-up period of 10 years starting in 1995 to stabilize Hg levels. We have used the inventory for speciated natural and anthropogenic Hg emissions from Zhang *et al.* (*87*) (representative for the year 2010) described above. This model setup is based on the Chemistry-Climate Model Initiative REFC1SD (Reference configuration with prescribed ocean and Specified Dynamics) experiment (*94*).

2) Present-day scenario with NH emissions: identical to the simulation of present-day scenario but implementing Hg emissions only in the Northern Hemisphere.

3) Future RCP8.5 2080–2099 scenario: future projection under the RCP8.5 scenario representing the 2090–2099 period (with a

spin-up of 10 years starting in 2080), assuming present-day global Hg emissions. Because future Hg emissions were not included, this simulation predicts changes in the Hg distribution attributable only to changes in atmospheric dynamics by the end of the 21st century in response to the RCP8.5 climate change scenario. The model setup is based on the REFC1 experiment (*94*), using sea surface temperature and sea ice field from a 2080–2099 REFC2 (Reference configuration with coupled ocean and free running) simulation.

Model validation

The model output has been thoroughly compared with available observations. Comparison with vertical profile observations of Hg(0) and Hg(I, II) atmospheric concentrations from previous studies, predominantly in the 30°N to 60°N region, is shown in Fig. 1D. In addition to vertical profiles, the surface Hg(0) estimates were validated using ground-based observations of Hg(0) from various globally distributed stations (fig. S9). Mercury deposition fluxes were compared with observations of wet deposition from several stations worldwide (fig. S11).

The dataset of Hg(0), Hg(I, II), and Hg(P) wet deposition observations used in this work is based on the compilation by Travnikov *et al.* (*46*). This dataset includes observations from the Global Mercury Observation System monitoring network (*37*, *95*), the European Monitoring and Evaluation Programme regional network (*96*), the Mercury Deposition Network of the National Atmospheric Deposition Program (*97*), the Atmospheric Mercury Network (*98*), and the Canadian National Atmospheric Chemistry Database (*99*, *100*). Annual mean measurements of Hg(0), Hg(II), and Hg(II) wet deposition flux in 2013 are included in the observation datasets. The location of all measurement sites is shown in fig. S10.

Hg(I, II) profiles are based on Northern Hemisphere midlatitude (30°N to 60°N) aircraft Hg(I, II) observations, using dual-channel oxidized Hg difference methods (*17*, *101*, *102*). Gaseous oxidized Hg(I, II) observations made by KCl-coated denuder methods (*103*) were multiplied by 1.56 according to Marusczak *et al.* (*104*) for typically observed denuder Hg(I, II) loss under dry free tropospheric conditions (*102*, *104*). Gaseous oxidized Hg(I, II) (loss corrected) and particulate Hg(I, II) in the Brooks *et al.* (*104*) study were summed to yield total Hg(I, II). The unique, but uncalibrated, stratospheric mean Hg(I, II) observations by Murphy *et al.* (*15*) were anchored to the Slemr *et al.* (*18*) mean Hg(I, II) observations for December to May (30°N to 60°N). All available aircraft Hg(I, II) data (*14*, *17*, *18*, *102*, *103*, *105*) were subsequently binned for 1-km altitude levels. Note that recent studies suggest that most, if not all, existing Hg(I, II) measurement techniques suffer from variable biases, depending on the local conditions and techniques used (*13*). Typically, oxidized Hg(I, II) observations are underestimated due to Hg loss from the sorbent surfaces (KCl-coated denuders, quartz wool, or cation exchange membranes). While we try to correct for some of this bias under dry free tropospheric conditions, such a correction provides a lower estimate for atmospheric Hg(I, II) at best.

For validation of the Hg(0) vertical profiles, we used aircraft observations over northern Europe from the European Tropospheric Mercury Experiment (ETMEP), which measured Hg(0) concentrations in a range of 500 to 3500 m (*25*, *106*), and the CARIBIC project (*107*, *108*), which measured total Hg and Hg(0) at altitudes from 6 to 12 km using a Tekran 2537A (*107*, *108*). The measurements in the ETMEP campaign were performed with two collocated Tekran instruments (2537X and 2537B), both operated with upstream particle filters and one (2537B) with an additional quartz wool trap to remove oxidized Hg species (*17*, *109*).

Model uncertainties

WACCM4 includes the most recent mercury redox atmospheric chemistry and photochemistry (*2*, *23*, *28*, *51*). The largest uncertainty contribution to the model results arises from the variability of kinetic and spectroscopic parameters of mercury reactions and compounds, as noted previously (*110*). In the case of the thermal reactions, we assume a rate coefficient uncertainty of ±25%, if error information from the original sources was lacking. In photochemical reactions, the largest uncertainty arises from the absorption coefficients of the spectra. We use here the spectra computed in our previous work (*2*, *23*, *28*, *51*), with an estimated ±25% uncertainty in the absorption cross sections, as discussed there. However, we acknowledge that the uncertainty to the model results can be larger than ±25%.

An additional source of uncertainty in the model results of deposited mercury is associated to the variability in mercury emission inventories, which for some sources are notoriously difficult to establish. However, this factor would not modify appreciably the main outcome of the present work. Different inventories would change the amount of surface-deposited mercury but would leave virtually unchanged the relative contribution of the stratosphere to mercury deposition. We remark that the specific emission inventory used in this work (*87*) results in good agreement with surface mercury observations (fig. S9). We also note that modeled mercury deposition values are time averages and, therefore, do not yield direct information on possible interannual variability. However, the annual variability is very weak in the time period studied here, as shown in fig. S12, and does not increase significantly the results' uncertainty. Note that, here, WACCM4 runs with specified dynamics, including reanalysis data for temperature, zonal and meridional winds, as well as surface pressure fields from MERRA2 (*65*–*67*).

Supplementary Materials

This PDF file includes:

Figs. S1 to S12
Tables S1 to S4
References

REFERENCES AND NOTES

1. UNEP-WCMC, IUCN, NGS, "Protected planet report 2018" (UNEP-WCMC, IUCN, NGS, 2018).
2. A. Saiz-Lopez, O. Travnikov, J. E. Sonke, C. P. Thackray, D. J. Jacob, J. Carmona-García, A. Francés-Monerris, D. Roca-Sanjuán, A. U. Acuña, J. Z. Dávalos, C. A. Cuevas, M. Jiskra, F. Wang, J. Bieser, J. M. C. Plane, J. S. Francisco, Photochemistry of oxidized Hg(I) and Hg(II) species suggests missing mercury oxidation in the troposphere. *Proc. Natl. Acad. Sci. U.S.A.* **117**, 30949–30956 (2020).
3. V. Shah, D. J. Jacob, C. P. Thackray, X. Wang, E. M. Sunderland, T. S. Dibble, A. Saiz-Lopez, I. Černušák, V. Kellö, P. J. Castro, R. Wu, C. Wang, Improved mechanistic model of the atmospheric redox chemistry of mercury. *Environ. Sci. Technol.* **55**, 14445–14456 (2021).
4. V. Shah, L. Jaeglé, Subtropical subsidence and surface deposition of oxidized mercury produced in the free troposphere. *Atmos. Chem. Phys.* **17**, 8999–9017 (2017).
5. United Nations Environment, "Minamata Convention on Mercury—Text and Annexes" (United Nations Environment, 2017).
6. S. N. Lyman, I. Cheng, L. E. Gratz, P. Weiss-Penzias, L. Zhang, An updated review of atmospheric mercury. *Sci. Total Environ.* **707**, 135575 (2020).
7. P. A. Ariya, M. Amyot, A. Dastoor, D. Deeds, A. Feinberg, G. Kos, A. Poulain, A. Ryjkov, K. Semeniuk, M. Subir, K. Toyota, Mercury physicochemical and biogeochemical

transformation in the atmosphere and at atmospheric interfaces: A review and future directions. *Chem. Rev.* **115**, 3760–3802 (2015).
8. F. Sprovieri, N. Pirrone, R. Ebinghaus, H. Kock, A. Dommergue, A review of worldwide atmospheric mercury measurements. *Atmos. Chem. Phys.* **10**, 8245–8265 (2010).
9. M. S. Gustin, S. M. Dunham-Cheatham, J. Huang, S. Lindberg, S. N. Lyman, Development of an understanding of reactive mercury in ambient air: A review. *Atmos.* **12**, 73 (2021).
10. A. Luippold, M. S. Gustin, S. M. Dunham-Cheatham, M. Castro, W. Luke, S. Lyman, L. Zhang, Use of multiple lines of evidence to understand reactive mercury concentrations and chemistry in Hawai'i, Nevada, Maryland, and Utah, USA. *Environ. Sci. Technol.* **54**, 7922–7931 (2020).
11. L. Zhang, P. Zhou, S. Cao, Y. Zhao, Atmospheric mercury deposition over the land surfaces and the associated uncertainties in observations and simulations: A critical review. *Atmos. Chem. Phys.* **19**, 15587–15608 (2019).
12. Z. Ye, H. Mao, C. Lin, Investigation of processes controlling GEM oxidation at mid-latitudinal marine, coastal, and inland sites. *Atmos. Chem. Phys. Discuss.* 10.5194/acp-2015-829 , (2016).
13. M. S. Gustin, S. M. Dunham-Cheatham, S. Lyman, M. Horvat, D. A. Gay, J. Gačnik, L. Gratz, G. Kempkes, A. Khalizov, C.-J. Lin, S. E. Lindberg, L. Lown, L. Martin, R. P. Mason, K. MacSween, S. V. Nair, L. S. P. Nguyen, T. O'Neil, J. Sommar, P. Weiss-Penzias, L. Zhang, I. Živković, Measurement of atmospheric mercury: Current limitations and suggestions for paths forward. *Environ. Sci. Technol.* **58**, 12853–12864 (2024).
14. D. M. Murphy, D. S. Thomson, M. J. Mahoney, In situ measurements of organics, meteoritic material, mercury, and other elements in aerosols at 5 to 19 kilometers. *Science* **282**, 1664–1669 (1998).
15. D. M. Murphy, P. K. Hudson, D. S. Thomson, P. J. Sheridan, J. C. Wilson, Observations of mercury-containing aerosols. *Environ. Sci. Technol.* **40**, 3163–3167 (2006).
16. R. Talbot, H. Mao, E. Scheuer, J. Dibb, M. Avery, Total depletion of Hg° in the upper troposphere-lower stratosphere. *Geophys. Res. Lett.* **34**, L23804 (2007).
17. S. N. Lyman, D. A. Jaffe, Formation and fate of oxidized mercury in the upper troposphere and lower stratosphere. *Nat. Geosci.* **5**, 114–117 (2012).
18. F. Slemr, A. Weigelt, R. Ebinghaus, J. Bieser, C. A. M. Brenninkmeijer, A. Rauthe-Schöch, M. Hermann, B. G. Martinsson, P. Van Velthoven, H. Bönisch, M. Neumaier, A. Zahn, H. Ziereis, Mercury distribution in the upper troposphere and lowermost stratosphere according to measurements by the IAGOS-CARIBIC observatory: 2014-2016. *Atmos. Chem. Phys.* **18**, 12329–12343 (2018).
19. N. E. Selin, D. J. Jacob, R. M. Yantosca, S. Strode, L. Jaeglé, E. M. Sunderland, Global 3-D land-ocean-atmosphere model for mercury: Present-day versus preindustrial cycles and anthropogenic enrichment factors for deposition. *Global Biogeochem. Cycles* **22**, GB2011 (2008).
20. C. D. Holmes, D. J. Jacob, X. Yang, Global lifetime of elemental mercury against oxidation by atomic bromine in the free troposphere. *Geophys. Res. Lett.* **33**, L20808 (2006).
21. A. J. Hynes, D. L. Donohoue, M. E. Goodsite, I. M. Hedgecock, in *Mercury Fate and Transport in the Global Atmosphere: Emissions, Measurements and Models*, R. Mason, N. Pirrone, Eds. (Springer, 2009), pp. 427–457; https://doi.org/10.1007/978-0-387-93958-2_14.
22. F. Wang, A. Saiz-Lopez, A. S. Mahajan, J. C. Gómez Martín, D. Armstrong, M. Lemes, T. Hay, C. Prados-Roman, Enhanced production of oxidised mercury over the tropical Pacific Ocean: A key missing oxidation pathway. *Atmos. Chem. Phys.* **14**, 1323–1335 (2014).
23. A. Francés-Monerris, J. Carmona-García, A. U. Acuña, J. Z. Dávalos, C. A. Cuevas, D. E. Kinnison, J. S. Francisco, A. Saiz-Lopez, D. Roca-Sanjuán, Photodissociation mechanisms of major mercury(II) species in the atmospheric chemical cycle of mercury. *Angew. Chemie Int. Ed.* **59**, 7605–7610 (2020).
24. H. M. Horowitz, D. J. Jacob, Y. Zhang, T. S. Dibble, F. Slemr, H. M. Amos, J. A. Schmidt, E. S. Corbitt, E. A. Marais, E. M. Sunderland, A new mechanism for atmospheric mercury redox chemistry: Implications for the global mercury budget. *Atmos. Chem. Phys.* **17**, 6353–6371 (2017).
25. J. Bieser, F. Slemr, J. Ambrose, C. Brenninkmeijer, S. Brooks, A. Dastoor, F. DeSimone, R. Ebinghaus, C. N. Gencarelli, B. Geyer, L. E. Gratz, I. M. Hedgecock, D. Jaffe, P. Kelley, C.-J. Lin, L. Jaegle, V. Matthias, A. Ryjkov, N. E. Selin, S. Song, O. Travnikov, A. Weigelt, W. Luke, X. Ren, A. Zahn, X. Yang, Y. Zhu, N. Pirrone, Multi-model study of mercury dispersion in the atmosphere: Vertical and interhemispheric distribution of mercury species. *Atmos. Chem. Phys.* **17**, 6925–6955 (2017).
26. A. Saiz-Lopez, A. U. Acuña, A. S. Mahajan, J. Z. Dávalos, W. Feng, D. Roca-Sanjuán, J. Carmona-García, C. A. Cuevas, D. E. Kinnison, J. C. Gómez Martín, J. S. Francisco, J. M. C. Plane, The chemistry of mercury in the stratosphere. *Geophys. Res. Lett.* **49**, e2022GL097953 (2022).
27. C. D. Holmes, D. J. Jacob, E. S. Corbitt, J. Mao, X. Yang, R. Talbot, F. Slemr, Global atmospheric model for mercury including oxidation by bromine atoms. *Atmos. Chem. Phys.* **10**, 12037–12057 (2010).
28. A. Saiz-Lopez, S. P. Sitkiewicz, D. Roca-Sanjuán, J. M. Oliva-Enrich, J. Z. Dávalos, R. Notario, M. Jiskra, Y. Xu, F. Wang, C. P. Thackray, E. M. Sunderland, D. J. Jacob, O. Travnikov, C. A. Cuevas, A. U. Acuña, D. Rivero, J. M. C. Plane, D. E. Kinnison, J. E. Sonke, Photoreduction of gaseous oxidized mercury changes global atmospheric mercury speciation, transport and deposition. *Nat. Commun.* **9**, 4796 (2018).
29. J. C. Gomez Martin, T. R. Lewis, K. M. Douglas, M. Blitz, A. Saiz-Lopez, J. M. C. Plane, The reaction between HgBr and O_3: Kinetic study and atmospheric implications. *Phys. Chem. Chem. Phys.* **24**, 12419–12432 (2022).
30. J. R. Holton, P. H. Haynes, M. E. McIntyre, A. R. Douglass, R. B. Rood, L. Pfister, Stratosphere-troposphere exchange. *Rev. Geophys.* **33**, 403–439 (1995).
31. S. Osterwalder, S. M. Dunham-Cheatham, B. F. Araujo, O. Magand, J. L. Thomas, F. Baladima, K. A. Pfaffhuber, T. Berg, L. Zhang, J. Huang, A. Dommergue, J. E. Sonke, M. S. Gustin, Fate of springtime atmospheric reactive mercury: Concentrations and deposition at Zeppelin, Svalbard. *ACS Earth Space Chem.* **5**, 3234–3246 (2021).
32. J. Bin Chen, H. Hintelmann, X. Bin Feng, B. Dimock, Unusual fractionation of both odd and even mercury isotopes in precipitation from Peterborough, ON, Canada. *Geochim. Cosmochim. Acta* **90**, 33–46 (2012).
33. C. Mead, J. R. Lyons, T. M. Johnson, A. D. Anbar, Unique Hg stable isotope signatures of compact fluorescent lamp-sourced Hg. *Environ. Sci. Technol.* **47**, 2542–2547 (2013).
34. G. Sun, X. Feng, R. Yin, F. Wang, C.-J. Lin, K. Li, J. O. Sommar, Dissociation of mercuric oxides drives anomalous isotope fractionation during net photo-oxidation of mercury vapor in air. *Environ. Sci. Technol.* **56**, 13428–13438 (2022).
35. X. Fu, M. Jiskra, X. Yang, N. Marusczak, M. Enrico, J. Chmeleff, L.-E. Heimbürger-Boavida, F. Gheusi, J. E. Sonke, Mass-independent fractionation of even and odd mercury isotopes during atmospheric mercury redox reactions. *Environ. Sci. Technol.* **55**, 10164–10174 (2021).
36. D. Obrist, J. L. Kirk, L. Zhang, E. M. Sunderland, M. Jiskra, N. E. Selin, A review of global environmental mercury processes in response to human and natural perturbations: Changes of emissions, climate, and land use. *Ambio* **47**, 116–140 (2018).
37. F. Sprovieri, N. Pirrone, M. Bencardino, F. D'Amore, F. Carbone, S. Cinnirella, V. Mannarino, M. Landis, R. Ebinghaus, A. Weigelt, E. G. Brunke, C. Labuschagne, L. Martin, J. Munthe, I. Wängberg, P. Artaxo, F. Morais, H. De Melo Jorge Barbosa, J. Brito, W. Cairns, C. Barbante, M. Del Carmen Diéguez, P. E. Garcia, D. Aurélien, H. Angot, O. Magand, H. Skov, M. Horvat, J. Kotnik, K. A. Read, L. Mendes Neves, B. Manfred Gawlik, F. Sena, N. Mashyanov, V. Obolkin, D. Wip, X. Bin Feng, H. Zhang, X. Fu, R. Ramachandran, D. Cossa, J. Knoery, N. Marusczak, M. Nerentorp, C. Norstrom, Atmospheric mercury concentrations observed at ground-based monitoring sites globally distributed in the framework of the GMOS network. *Atmos. Chem. Phys.* **16**, 11915–11935 (2016).
38. D. G. Streets, H. M. Horowitz, D. J. Jacob, Z. Lu, L. Levin, A. F. H. ter Schure, E. M. Sunderland, Total mercury released to the environment by human activities. *Environ. Sci. Technol.* **51**, 5969–5977 (2017).
39. A. M. Koenig, J. E. Sonke, O. Magand, M. Andrade, I. Moreno, F. Velarde, R. Forno, R. Gutierrez, L. Blacutt, P. Laj, P. Ginot, J. Bieser, A. Zahn, F. Slemr, A. Dommergue, Evidence for interhemispheric mercury exchange in the Pacific Ocean upper troposphere. *J. Geophys. Res. Atmos.* **127**, e2021JD036283 (2022).
40. R. R. Garcia, W. J. Randel, Acceleration of the brewer-dobson circulation due to increases in greenhouse gases. *J. Atmos. Sci.* **65**, 2731–2739 (2008).
41. T. G. Shepherd, C. McLandress, A robust mechanism for strengthening of the Brewer–Dobson circulation in response to climate change: Critical-layer control of subtropical wave breaking. *J. Atmos. Sci.* **68**, 784–797 (2011).
42. P. Šácha, R. Eichinger, H. Garny, P. Pišoft, S. Dietmüller, L. de la Torre, D. A. Plummer, P. Jöckel, O. Morgenstern, G. Zeng, N. Butchart, J. A. Añel, Extratropical age of air trends and causative factors in climate projection simulations. *Atmos. Chem. Phys.* **19**, 7627–7647 (2019).
43. M. Meinshausen, S. J. Smith, K. Calvin, J. S. Daniel, M. L. T. Kainuma, J.-F. Lamarque, K. Matsumoto, S. A. Montzka, S. C. B. Raper, K. Riahi, A. Thomson, G. J. M. Velders, D. P. P. van Vuuren, The RCP greenhouse gas concentrations and their extensions from 1765 to 2300. *Clim. Change* **109**, 213–241 (2011).
44. F. De Simone, F. D'Amore, F. Marasco, F. Carbone, M. Bencardino, I. M. Hedgecock, S. Cinnirella, F. Sprovieri, N. Pirrone, A chemical transport model emulator for the interactive evaluation of mercury emission reduction scenarios. *Atmos.* **11**, 878 (2020).
45. K. M. Mulvaney, N. E. Selin, A. Giang, M. Muntean, C.-T. Li, D. Zhang, H. Angot, C. P. Thackray, V. J. Karplus, Mercury benefits of climate policy in China: Addressing the Paris agreement and the minamata convention simultaneously. *Environ. Sci. Technol.* **54**, 1326–1335 (2020).
46. O. Travnikov, H. Angot, P. Artaxo, M. Bencardino, J. Bieser, F. D'Amore, A. Dastoor, F. De Simone, M. C. Dléguez, A. Dommergue, R. Ebinghaus, X. B. Feng, C. N. Gencarelli, I. M. Hedgecock, O. Magand, L. Martin, V. Matthias, N. Mashyanov, N. Pirrone, R. Ramachandran, K. A. Read, A. Ryjkov, N. E. Selin, F. Sena, S. Song, F. Sprovieri, D. Wip, I. Wängberg, X. Yang, Multi-model study of mercury dispersion in the atmosphere: Atmospheric processes and model evaluation. *Atmos. Chem. Phys.* **17**, 5271–5295 (2017).
47. R. Wu, C. Wang, T. S. Dibble, First experimental kinetic study of the atmospherically important reaction of BrHg + NO2. *Chem. Phys. Lett.* **759**, 137928 (2020).
48. K. T. Lam, C. J. Wilhelmsen, A. C. Schwid, Y. Jiao, T. S. Dibble, Computational study on the photolysis of BrHgONO and the reactions of BrHgO with CH_4, C_2H_6, NO, and NO_2:

Implications for formation of Hg(II) compounds in the atmosphere. *J. Phys. Chem. A* **123**, 1637–1647 (2019).
49. D. Khiri, F. Louis, I. Černušák, T. S. Dibble, BrHgO˙ + CO: Analogue of OH + CO and reduction path for Hg(II) in the atmosphere. *ACS Earth Space Chem.* **4**, 1777–1784 (2020).
50. S. P. Sitkiewicz, D. Rivero, J. M. Oliva-Enrich, A. Saiz-Lopez, D. Roca-Sanjuán, Ab initio quantum-chemical computations of the absorption cross sections of HgX2 and HgXY (X, Y= Cl, Br, and I): Molecules of interest in the Earth's atmosphere. *Phys. Chem. Chem. Phys.* **21**, 455–467 (2019).
51. A. Saiz-Lopez, A. U. Acuña, T. Trabelsi, J. Carmona-García, J. Z. Dávalos, D. Rivero, C. A. Cuevas, D. E. Kinnison, S. P. Sitkiewicz, D. Roca-Sanjuán, J. S. Francisco, Gas-phase photolysis of Hg(I) radical species: A new atmospheric mercury reduction process. *J. Am. Chem. Soc.* **141**, 8698–8702 (2019).
52. L. Zhang, L. P. Wright, P. Blanchard, A review of current knowledge concerning dry deposition of atmospheric mercury. *Atmos. Environ.* **43**, 5853–5864 (2009).
53. J. L. Neu, M. J. Prather, Toward a more physical representation of precipitation scavenging in global chemistry models: Cloud overlap and ice physics and their impact on tropospheric ozone. *Atmos. Chem. Phys.* **12**, 3289–3310 (2012).
54. R. Sander, Compilation of Henry's law constants (version 4.0) for water as solvent. *Atmos. Chem. Phys.* **15**, 4399–4981 (2015).
55. WMO, World Meteorological Organization, *Meteorology—A three-dimensional science: Second session of the commission for aerology*, *WMO Bull.* **4**, 134–138 (1957).
56. T. Reichler, M. Dameris, R. Sausen, Determining the tropopause height from gridded data. *Geophys. Res. Lett.* **30**, 2042 (2003).
57. C. Appenzeller, J. R. Holton, K. H. Rosenlof, Seasonal variation of mass transport across the tropopause. *J. Geophys. Res. Atmos.* **101**, 15071–15078 (1996).
58. D. G. Andrews, M. E. McIntyre, Planetary waves in horizontal and vertical shear: The generalized Eliassen-Palm relation and the mean zonal acceleration. *J. Atmos. Sci.* **33**, 2031–2048 (1976).
59. D. G. Andrews, M. E. McIntyre, Generalized Eliassen-Palm and Charney-Drazin theorems for waves on axismmetric mean flows in compressible atmospheres. *J. Atmos. Sci.* **35**, 175–185 (1978).
60. K. H. Rosenlof, Seasonal cycle of the residual mean meridional circulation in the stratosphere. *J. Geophys. Res. Atmos.* **100**, 5173–5191 (1995).
61. A. C. Boothe, C. R. Homeyer, Global large-scale stratosphere–troposphere exchange in modern reanalyses. *Atmos. Chem. Phys.* **17**, 5537–5559 (2017).
62. B. Škerlak, M. Sprenger, H. Wernli, A global climatology of stratosphere–troposphere exchange using the ERA-Interim data set from 1979 to 2011. *Atmos. Chem. Phys.* **14**, 913–937 (2014).
63. R. B. Neale, J. Richter, S. Park, P. H. Lauritzen, S. J. Vavrus, P. J. Rasch, M. Zhang, The mean climate of the community atmosphere model (CAM4) in forced SST and Fully coupled experiments. *J. Climate* **26**, 5150–5168 (2013).
64. V. Eyring, T. G. Shepherd, D. W. Waugh, "SPARC CCMVal report on the evaluation of chemistry-climate models" (SPARC Office, 2010); www.sparc-climate.org/publications/sparc-reports/.
65. R. Gelaro, W. McCarty, M. J. Suárez, R. Todling, A. Molod, L. Takacs, C. A. Randles, A. Darmenov, M. G. Bosilovich, R. Reichle, K. Wargan, L. Coy, R. Cullather, C. Draper, S. Akella, V. Buchard, A. Conaty, A. M. da Silva, W. Gu, G.-K. Kim, R. Koster, R. Lucchesi, D. Merkova, J. E. Nielsen, G. Partyka, S. Pawson, W. Putman, M. Rienecker, S. D. Schubert, M. Sienkiewicz, B. Zhao, The Modern-Era Retrospective Analysis for Research and Applications, version 2 (MERRA-2). *J. Climate* **30**, 5419–5454 (2017).
66. M. M. Rienecker, M. J. Suarez, R. Gelaro, R. Todling, J. Bacmeister, E. Liu, M. G. Bosilovich, S. D. Schubert, L. Takacs, G.-K. Kim, S. Bloom, J. Chen, D. Collins, A. Conaty, A. da Silva, W. Gu, J. Joiner, R. D. Koster, R. Lucchesi, A. Molod, T. Owens, S. Pawson, P. Pegion, C. R. Redder, R. Reichle, F. R. Robertson, A. G. Ruddick, M. Sienkiewicz, J. Woollen, MERRA: NASA's Modern-Era Retrospective Analysis for Research and Applications. *J. Climate* **24**, 3624–3648 (2011).
67. R. R. Garcia, A. K. Smith, D. E. Kinnison, Á. de la Cámara, D. J. Murphy, Modification of the gravity wave parameterization in the whole atmosphere community climate model: Motivation and results. *J. Atmos. Sci.* **74**, 275–291 (2017).
68. JPL, "Chemical kinetics and photochemical data for use in atmospheric studies" (Evaluation Number 17, JPL Publ. 10-6, Jet Propulsion Laboratory, 2011).
69. A. Saiz-Lopez, R. P. Fernandez, Q. Li, C. A. Cuevas, X. Fu, D. E. Kinnison, S. Tilmes, A. S. Mahajan, J. C. Martín Gómez, F. Iglesias-Suarez, R. Hossaini, J. M. C. Plane, G. Myhre, J.-F. Lamarque, Natural short-lived halogens exert an indirect cooling effect on climate. *Nature* **618**, 967–973 (2023).
70. C. A. Cuevas, R. P. Fernandez, D. E. Kinnison, Q. Li, J.-F. Lamarque, T. Trabelsi, J. S. Francisco, S. Solomon, A. Saiz-Lopez, The influence of iodine on the Antarctic stratospheric ozone hole. *Proc. Natl. Acad. Sci. U.S.A.* **119**, e2110864119 (2022).
71. M. Park, W. J. Randel, D. E. Kinnison, L. K. Emmons, P. F. Bernath, K. A. Walker, C. D. Boone, N. J. Livesey, Hydrocarbons in the upper troposphere and lower stratosphere observed from ACE-FTS and comparisons with WACCM. *J. Geophys. Res. Atmos.* **118**, 1964–1980 (2013).
72. M. Abalos, W. J. Randel, D. E. Kinnison, R. R. Garcia, Using the artificial tracer e90 to examine present and future UTLS tracer transport in WACCM. *J. Atmos. Sci.* **74**, 3383–3403 (2017).
73. M. Abalos, C. Orbe, D. E. Kinnison, D. Plummer, L. D. Oman, P. Jöckel, O. Morgenstern, R. R. Garcia, G. Zeng, K. A. Stone, M. Dameris, Future trends in stratosphere-to-troposphere transport in CCMI models. *Atmos. Chem. Phys.* **20**, 6883–6901 (2020).
74. H. Yang, G. Chen, Q. Tang, P. Hess, Quantifying isentropic stratosphere-troposphere exchange of ozone. *J. Geophys. Res. Atmos.* **121**, 3372–3387 (2016).
75. D. Minganti, S. Chabrillat, Y. Christophe, Q. Errera, M. Abalos, M. Prignon, D. E. Kinnison, E. Mahieu, Climatological impact of the Brewer–Dobson circulation on the N_2O budget in WACCM, a chemical reanalysis and a CTM driven by four dynamical reanalyses. *Atmos. Chem. Phys.* **20**, 12609–12631 (2020).
76. K. Shah, S. Solomon, D. Kinnison, Q. Fu, D. W. J. Thompson, Phase unlocking and the modulation of tropopause-level trace gas advection by the quasibiennial oscillation. *J. Geophys. Res. Atmos.* **127**, e2021JD036142 (2022).
77. A. Banerjee, A. C. Maycock, A. T. Archibald, N. L. Abraham, P. Telford, P. Braesicke, J. A. Pyle, Drivers of changes in stratospheric and tropospheric ozone between year 2000 and 2100. *Atmos. Chem. Phys.* **16**, 2727–2746 (2016).
78. C. Ordóñez, J.-F. Lamarque, S. Tilmes, D. E. Kinnison, E. L. Atlas, D. R. Blake, G. Sousa Santos, G. Brasseur, A. Saiz-Lopez, Bromine and iodine chemistry in a global chemistry-climate model: Description and evaluation of very short-lived oceanic sources. *Atmos. Chem. Phys.* **12**, 1423–1447 (2012).
79. R. P. Fernandez, R. J. Salawitch, D. E. Kinnison, J.-F. Lamarque, A. Saiz-Lopez, Bromine partitioning in the tropical tropopause layer: Implications for stratospheric injection. *Atmos. Chem. Phys.* **14**, 13391–13410 (2014).
80. A. Saiz-Lopez, R. P. Fernandez, C. Ordóñez, D. E. Kinnison, J. C. Gómez Martín, J.-F. Lamarque, S. Tilmes, Iodine chemistry in the troposphere and its effect on ozone. *Atmos. Chem. Phys.* **14**, 13119–13143 (2014).
81. J. A. Barrera, R. P. Fernandez, F. Iglesias-Suarez, C. A. Cuevas, J.-F. Lamarque, A. Saiz-Lopez, Seasonal impact of biogenic very short-lived bromocarbons on lowermost stratospheric ozone between 60°N and 60°S during the 21st century. *Atmos. Chem. Phys.* **20**, 8083–8102 (2020).
82. R. P. Fernandez, D. E. Kinnison, J. F. Lamarque, S. Tilmes, A. Saiz-Lopez, Impact of biogenic very short-lived bromine on the Antarctic ozone hole during the 21st century. *Atmos. Chem. Phys.* **17**, 1673–1688 (2017).
83. C. Prados-Roman, C. A. Cuevas, R. P. Fernandez, D. E. Kinnison, J.-F. Lamarque, A. Saiz-Lopez, A negative feedback between anthropogenic ozone pollution and enhanced ocean emissions of iodine. *Atmos. Chem. Phys.* **15**, 2215–2224 (2015).
84. F. Iglesias-Suarez, A. Badia, R. P. Fernandez, C. A. Cuevas, D. E. Kinnison, S. Tilmes, J.-F. Lamarque, M. C. Long, R. Hossaini, A. Saiz-Lopez, Natural halogens buffer tropospheric ozone in a changing climate. *Nat. Clim. Chang.* **10**, 147–154 (2020).
85. S. M. MacDonald, J. C. Gómez Martín, R. Chance, S. Warriner, A. Saiz-Lopez, L. J. Carpenter, J. M. C. Plane, A laboratory characterisation of inorganic iodine emissions from the sea surface: Dependence on oceanic variables and parameterisation for global modelling. *Atmos. Chem. Phys.* **14**, 5841–5852 (2014).
86. L. J. Carpenter, S. M. MacDonald, M. D. Shaw, R. Kumar, R. W. Saunders, R. Parthipan, J. Wilson, J. M. C. Plane, Atmospheric iodine levels influenced by sea surface emissions of inorganic iodine. *Nat. Geosci.* **6**, 108–111 (2013).
87. Y. Zhang, D. J. Jacob, H. M. Horowitz, L. Chen, H. M. Amos, D. P. Krabbenhoft, F. Slemr, V. L. St. Louis, E. M. Sunderland, Observed decrease in atmospheric mercury explained by global decline in anthropogenic emissions. *Proc. Natl. Acad. Sci. U.S.A.* **113**, 526–531 (2016).
88. Y. Zhang, D. J. Jacob, S. Dutkiewicz, H. M. Amos, M. S. Long, E. M. Sunderland, Biogeochemical drivers of the fate of riverine mercury discharged to the global and Arctic oceans. *Global Biogeochem. Cycles* **29**, 854–864 (2015).
89. Y. Zhang, P. Zhang, Z. Song, S. Huang, T. Yuan, P. Wu, V. Shah, M. Liu, L. Chen, X. Wang, J. Zhou, Y. Agnan, An updated global mercury budget from a coupled atmosphere-land-ocean model: 40% more re-emissions buffer the effect of primary emission reductions. *One Earth* **6**, 316–325 (2023).
90. G. W. Evatt, A. R. D. Smedley, K. H. Joy, L. Hunter, W. H. Tey, I. D. Abrahams, L. Gerrish, The spatial flux of Earth's meteorite falls found via Antarctic data. *Geology* **48**, 683–687 (2020).
91. F. Moynier, J. Chen, K. Zhang, H. Cai, Z. Wang, M. G. Jackson, J. M. D. Day, Chondritic mercury isotopic composition of Earth and evidence for evaporative equilibrium degassing during the formation of eucrites. *Earth Planet. Sci. Lett.* **551**, 116544 (2020).
92. M. M. M. Meier, C. Cloquet, B. Marty, Mercury (Hg) in meteorites: Variations in abundance, thermal release profile, mass-dependent and mass-independent isotopic fractionation. *Geochim. Cosmochim. Acta* **182**, 55–72 (2016).
93. M. Asplund, N. Grevesse, A. J. Sauval, P. Scott, The chemical composition of the sun. *Annu. Rev. Astron. Astrophys.* **47**, 481–522 (2009).
94. S. Tilmes, J. F. Lamarque, L. K. Emmons, D. E. Kinnison, D. Marsh, R. R. Garcia, A. K. Smith, R. R. Neely, A. Conley, F. Vitt, M. Val Martin, H. Tanimoto, I. Simpson, D. R. Blake, N. Blake,

Representation of the Community Earth System Model (CESM1) CAM4-chem within the Chemistry-Climate Model Initiative (CCMI). *Geosci. Model Dev.* **9**, 1853–1890 (2016).
95. F. Sprovieri, N. Pirrone, M. Bencardino, F. D'Amore, H. Angot, C. Barbante, E.-G. Brunke, F. Arcega-Cabrera, W. Cairns, S. Comero, M. D. C. Diéguez, A. Dommergue, R. Ebinghaus, X. B. Feng, X. Fu, P. E. Garcia, B. M. Gawlik, U. Hageström, K. Hansson, M. Horvat, J. Kotnik, C. Labuschagne, O. Magand, L. Martin, N. Mashyanov, T. Mkololo, J. Munthe, V. Obolkin, M. Ramirez Islas, F. Sena, V. Somerset, P. Spandow, M. Vardè, C. Walters, I. Wängberg, A. Weigelt, X. Yang, H. Zhang, Five-year records of mercury wet deposition flux at GMOS sites in the Northern and Southern hemispheres. *Atmos. Chem. Phys.* **17**, 2689–2708 (2017).
96. K. Tørseth, W. Aas, K. Breivik, A. M. Fjæraa, M. Fiebig, A. G. Hjellbrekke, C. Lund Myhre, S. Solberg, K. E. Yttri, Introduction to the European Monitoring and Evaluation Programme (EMEP) and observed atmospheric composition change during 1972-2009. *Atmos. Chem. Phys.* **12**, 5447–5481 (2012).
97. E. M. Prestbo, D. A. Gay, Wet deposition of mercury in the U.S. and Canada, 1996–2005: Results and analysis of the NADP mercury deposition network (MDN). *Atmos. Environ.* **43**, 4223–4233 (2009).
98. D. A. Gay, D. Schmeltz, E. Prestbo, M. Olson, T. Sharac, R. Tordon, The Atmospheric Mercury Network: Measurement and initial examination of an ongoing atmospheric mercury record across North America. *Atmos. Chem. Phys.* **13**, 11339–11349 (2013).
99. A. S. Cole, A. Steffen, K. A. Pfaffhuber, T. Berg, M. Pilote, L. Poissant, R. Tordon, H. Hung, Ten-year trends of atmospheric mercury in the high Arctic compared to Canadian sub-Arctic and mid-latitude sites. *Atmos. Chem. Phys.* **13**, 1535–1545 (2013).
100. A. Steffen, I. Lehnherr, A. Cole, P. Ariya, A. Dastoor, D. Durnford, J. Kirk, M. Pilote, Atmospheric mercury in the Canadian Arctic. Part I: A review of recent field measurements. *Sci. Total Environ.* **509–510**, 3–15 (2015).
101. L. E. Gratz, J. L. Ambrose, D. A. Jaffe, V. Shah, L. Jaeglé, J. Stutz, J. Festa, M. Spolaor, C. Tsai, N. E. Selin, S. Song, X. Zhou, A. J. Weinheimer, D. J. Knapp, D. D. Montzka, F. M. Flocke, T. L. Campos, E. Apel, R. Hornbrook, N. J. Blake, S. Hall, G. S. Tyndall, M. Reeves, D. Stechman, M. Stell, Oxidation of mercury by bromine in the subtropical pacific free troposphere. *Geophys. Res. Lett.* **42**, 10494–10502 (2015).
102. P. C. Swartzendruber, D. A. Jaffe, B. Finley, Development and first results of an aircraft-based, high time resolution technique for gaseous elemental and reactive (oxidized) gaseous mercury. *Environ. Sci. Technol.* **43**, 7484–7489 (2009).
103. S. Brooks, X. Ren, M. Cohen, W. T. Luke, P. Kelley, R. Artz, A. Hynes, W. Landing, B. Martos, Airborne vertical profiling of mercury speciation near Tullahoma, TN, USA. *Atmos.* **5**, 557–574 (2014).
104. N. Marusczak, J. E. Sonke, X. Fu, M. Jiskra, Tropospheric GOM at the Pic du Midi Observatory—Correcting bias in denuder based observations. *Environ. Sci. Technol.* **51**, 863–869 (2017).
105. V. Shah, L. Jaeglé, L. E. Gratz, J. L. Ambrose, D. A. Jaffe, N. E. Selin, S. Song, T. L. Campos, F. M. Flocke, M. Reeves, D. Stechman, M. Stell, J. Festa, J. Stutz, A. J. Weinheimer, D. J. Knapp, D. D. Montzka, G. S. Tyndall, E. C. Apel, R. S. Hornbrook, A. J. Hills, D. D. Riemer, N. J. Blake, C. A. Cantrell, R. L. Mauldin III, Origin of oxidized mercury in the summertime free troposphere over the southeastern US. *Atmos. Chem. Phys.* **16**, 1511–1530 (2016).
106. A. Weigelt, R. Ebinghaus, N. Pirrone, J. Bieser, J. Bödewadt, G. Esposito, F. Slemr, P. F. J. van Velthoven, A. Zahn, H. Ziereis, Tropospheric mercury vertical profiles between 500 and 10 000 m in central Europe. *Atmos. Chem. Phys.* **16**, 4135–4146 (2016).
107. F. Slemr, A. Weigelt, R. Ebinghaus, H. H. Kock, J. Bödewadt, C. A. M. Brenninkmeijer, A. Rauthe-Schöch, S. Weber, M. Hermann, J. Becker, A. Zahn, B. Martinsson, Atmospheric mercury measurements onboard the CARIBIC passenger aircraft. *Atmos. Meas. Tech.* **9**, 2291–2302 (2016).
108. F. Slemr, A. Weigelt, R. Ebinghaus, C. Brenninkmeijer, A. Baker, T. Schuck, A. Rauthe-Schöch, H. Riede, E. Leedham, M. Hermann, P. Van Velthoven, D. Oram, D. O'Sullivan, C. Dyroff, A. Zahn, H. Ziereis, Mercury plumes in the global upper troposphere observed during flights with the CARIBIC Observatory from May 2005 until June 2013. *Atmos.* **5**, 342–369 (2014).
109. J. L. Ambrose, S. N. Lyman, J. Huang, M. S. Gustin, D. A. Jaffe, Fast time resolution oxidized mercury measurements during the reno atmospheric mercury intercomparison experiment (RAMIX). *Environ. Sci. Technol.* **47**, 7285–7294 (2013).
110. M. Subir, P. A. Ariya, A. P. Dastoor, A review of uncertainties in atmospheric modeling of mercury chemistry I. Uncertainties in existing kinetic parameters–Fundamental limitations and the importance of heterogeneous chemistry. *Atmos. Environ.* **45**, 5664–5676 (2011).
111. D. L. Donohoue, D. Bauer, B. Cossairt, A. J. Hynes, Temperature and pressure dependent rate coefficients for the reaction of Hg with Br and the reaction of Br with Br: A pulsed laser photolysis-pulsed laser induced fluorescence study. *J. Phys. Chem. A* **110**, 6623–6632 (2006).
112. B. Pal, P. A. Ariya, Gas-phase HO•-initiated reactions of elemental mercury: Kinetics, product studies, and atmospheric implications. *Environ. Sci. Technol.* **38**, 5555–5566 (2004).
113. D. L. Donohoue, D. Bauer, A. J. Hynes, Temperature and pressure dependent rate coefficients for the reaction of Hg with Cl and the reaction of Cl with Cl: A pulsed laser photolysis–pulsed laser induced fluorescence study. *J. Phys. Chem. A* **109**, 7732–7741 (2005).
114. T. S. Dibble, M. J. Zelie, H. Mao, Thermodynamics of reactions of ClHg and BrHg radicals with atmospherically abundant free radicals. *Atmos. Chem. Phys.* **12**, 10271–10279 (2012).
115. N. B. Balabanov, B. C. Shepler, K. A. Peterson, Accurate global potential energy surface and reaction dynamics for the ground state of HgBr2. *J. Phys. Chem. A* **109**, 8765–8773 (2005).
116. M. E. Goodsite, J. M. C. Plane, H. Skov, A theoretical study of the oxidation of Hg-0 to HgBr2 in the troposphere. *Environ. Sci. Technol.* **38**, 1772–1776 (2004).
117. Y. Jiao, T. S. Dibble, First kinetic study of the atmospherically important reactions $BrHg^{\cdot}$ + NO_2 and $BrHg^{\cdot}$ + HOO. *Phys. Chem. Chem. Phys.* **19**, 1826–1838 (2017).
118. T. S. Dibble, H. L. Tetu, Y. Jiao, C. P. Thackray, D. J. Jacob, Modeling the OH-initiated oxidation of mercury in the global atmosphere without violating physical laws. *J. Phys. Chem. A* **124**, 444–453 (2020).
119. A. Kramida, Y. Ralchenko, J. Reader, NIST ASD Team, Atomic Spectra Database, NIST Standard Reference Database 78 (2018); https://doi.org/10.18434/T4W30F.
120. A. B. Callear, P. M. Shiundu, Temperature dependence of the Hg 6s6p(3P0→3P1) transition induced by nitrogen. *Chem. Phys. Lett.* **136**, 342–345 (1987).
121. A. B. Callear, Excited mercury complexes. *Chem. Rev.* **87**, 335–355 (1987).

Acknowledgments: We are grateful to R. Garcia, M. Abalos, and N. Selin for helpful discussions. **Funding:** This work is funded by the European Research Council Executive Agency under Horizon 2020 Research and Innovation programme project ERC-2016-COG 726349 CLIMAHAL. J.A.A. and L.d.l.T. are supported by a grant from the Spanish State Research Agency (CHESS, PID2021-124991OB-I00). The EPhysLab is supported by the Government of Galicia (grant ED431C 2021/44). J.A.A.'s work at IQF-CSIC is supported by a grant from the Spanish Ministry of Universities and the Universidade de Vigo. The National Centre for Atmospheric Research (NCAR) is funded by the National Science Foundation (NSF). Computing resources were provided by the Climate Simulation Laboratory at NCAR's Computational and Information Systems Laboratory (CISL), sponsored by the NSF. The CESM project is supported by the NSF and the Office of Science (BER) of the US Department of Energy. R.P.F. appreciates the financial support from ANPCyT (PICT 2019-2187). IITM is funded by the Ministry of Earth Sciences, Government of India. We are grateful to NorArte Visual Science for the design of Fig. 3. A.F. is funded by the Swiss National Science Foundation (P2EZP2_195424), the US National Science Foundation (no. 1924148), and the Horizon Europe MSCA-PF (101103544). The project that gave rise to these results received the support of a fellowship for J.C.-G. from "la Caixa" Foundation (ID 100010434); the fellowship code is LCF/BQ/DR20/11790027. D.R.-S. and J.C.-G. are thankful to the Spanish Agencia Estatal de Investigación of the Ministerio de Ciencia e Innovación (MICINN) and the European Regional Development Fund (FEDER) through project no. PID2021-127199NB-I00, and the Generalitat Valenciana for funding via the project CIAICO/2022/121. **Author contributions:** Conceptualization: A.S.-L., J.M.C.P., A.U.A., J.B., and J.C.G.M. Methodology: A.S.-L., J.M.C.P., C.A.C., A.U.A., W.F., A.S.M., J.V., R.P.F., D.E.K., D.R.-S., J.C.-G., Y.Z., L.d.l.T., J.A.A., and Q.L. Investigation: A.S.-L., C.A.C., A.U.A., W.F., J.S.F., J.E.S., A.F., O.T., A.S.M., D.R.-S., L.d.l.T., J.C.G.M., J.A.A., J.Z.D., and F.W. Software: A.S.-L., C.A.C., R.P.F., Q.L., D.R.-S., L.d.l.T., D.E.K., W.F., and J.A.A. Data curation: A.S.-L., C.A.C., C.S.B.-B., and J.B. Formal analysis: A.S.-L., C.A.C., R.P.F., A.S.M., C.S.B.-B., Y.Z., L.d.l.T., J.E.S., and J.A.A. Validation: A.S.-L., C.A.C., J.E.S., D.R.-S., L.d.l.T., and J.A.A. Visualization: A.S.-L., C.A.C., J.A.A., L.d.l.T., A.U.A., and J.E.S. Funding acquisition: A.S.-L., D.R.-S., J.E.S., and J.A.A. Project administration: A.S.-L. and J.A.A. Resources: A.S.-L., A.U.A., D.R.-S., P.Z., Y.Z., J.B., L.d.l.T., J.Z.D., and J.A.A. Supervision: A.S.-L. and C.S.B.-B. Writing—original draft: A.S.-L., A.U.A., J.M.C.P., Y.Z., J.C.G.M., J.A.A., and A.S.M. Writing—review and editing: all authors. **Competing interests:** The authors declare that they have no competing interests. **Data and materials availability:** Data supporting this article are available at Mendeley Datasets (DOI: 10.17632/hsgdhkjtx3.1). The software code for the CESM model is available from www.cesm.ucar.edu/models/. All other data needed to evaluate the conclusions in the paper are present in the paper and/or the Supplementary Materials.

Submitted 31 July 2024
Accepted 4 December 2024
Published 8 January 2025
10.1126/sciadv.ads1459